J Fluoresc
DOI 10.1007/s10895-017-2135-x

ORIGINAL ARTICLE

Comparison of the Optoelectronic Performance of Neutral and Cationic Forms of Riboflavin

Gözde Murat Saltan[1] · **Deniz Aykut Kıymaz**[2] · **Ceylan Zafer**[2] · **Haluk Dinçalp**[1]

Received: 24 March 2017 / Accepted: 30 June 2017

Abstract The riboflavin dye 2,3,4,5-tetra-O-acetyl-1-[3-(6-bromohexyl)-7,8-dimethyl-2,4-dioxo-3,4-dihydrobenzo[g]pteridin-10(2H)-yl]-1-deoxypentitol and its pyridinium salt were synthesized, and studied by absorption and fluorescence spectroscopy in solutions and on thin film states. The first absorption band of riboflavin-pyridinium salt derivative is red-shifted by 10 nm compared to neutral one on film. Cationic riboflavin derivative shows significant wavelength changes on its fluorescence emission spectrum in the excited state depending on the solvent polarity and the electronic environment. The fluorescence quantum yields of cationic riboflavin gave much higher values as compared to that of its neutral form. The fluorescence lifetimes were found to be in the range of 5.5–6.6 ns with mono − exponential behavior. These dyes possess low-lying HOMO energy levels which are suitable to be able to inject holes to donor polymers so that they can be used as acceptor component in the active layer of bulk heterojunction solar cells (BHJ-SCs). Photovoltaic responses are reported for P3HT:riboflavin active layer wherein the synthesized dyes are used as acceptor component. Also, neutral riboflavin shows greater electron mobility value of 1.3×10^{-3} $cm^2/V \cdot s$ compared to its cationic derivative.

Keywords Optoelectronic materials · Riboflavin · Fluorescent · Thin films · Photovoltaic

Introduction

Riboflavin, also known as Vitamin B2, is a vitamin commonly found in plants and organisms, and often used as a photosensitizer in metabolic and photosynthetic processes [1, 2]. Isoalloxazine ring, which constitutes the basic structure of riboflavin, is the basic chromophore group that enriches for π electrons [3]. Flavin mononucleotide (FMN) biomolecule and flavin adenine dinucleotide (FAD) cofactor, the most popular phosphorylated forms of riboflavin, are involved in several flavoprotein enzyme reactions [4]. Riboflavin and its derivatives can undergo photodegradation reactions in organic solvents under visible light irradiation in an oxygenated or oxygen-free atmosphere, giving alloxazine and isoalloxazine fragmentations. In the literature, especially tetraacetyl derivatives of riboflavin have been prepared in order to increase its photostability. More specifically, 3-methyl-riboflavin tetraacetate derivatives are more stable than unsubstituted riboflavin structure [5].

Riboflavin and its natural or synthetic derivatives have a wide range of usages in food systems [6, 7], clinical and biomedical applications [8], photodynamic inactivation processes [9], photodynamic therapy applications [10, 11] and drugs [12]. Riboflavin dye was also used as a photosensitizer in dye sensitized solar cells consisting of indium tin oxide (ITO), zinc oxide (ZnO), polyaniline based-single [13] or multi walled carbon nanotube [14], giving satisfying cell efficiencies. In 2016, Mollahosseini et al. reported a multi material system composed of a C_{60}-functionalized isoalloxazine derivative and a flavin helix wrapped-single walled carbon nanotube structure was designed to increase photoinduced charge transfer quenching inside the system. This combination facilitates the $\pi - \pi$ overlap between the graphene sidewalls, isoalloxazine, and the C_{60} acceptor that enables the efficient

✉ Haluk Dinçalp
haluk.dincalp@cbu.edu.tr

[1] Department of Chemistry, Faculty of Arts and Science, Manisa Celal Bayar University, Yunus Emre, 45140 Manisa, Turkey

[2] Solar Energy Institute, Ege University, Bornova, 35100 Izmir, Turkey

electron transfer to the PCBM moiety [15]. Also, novel donor-acceptor type flavin dyads initiated an efficient electron transfer process that indicated the potential usage of flavin dyes as an acceptor molecule in photovoltaic applications [16, 17]. These results give us a clue that a BHJ-SC device containing riboflavin derivative in active layer may work properly.

Thus, photophysical and optoelectronic properties of riboflavin and its derivatives have been considered worthy of investigation in this regard. Besides, the riboflavin chromophore has a strong absorption band between 440 and 450 nm in solution depending on polarity of used solvent [10]. Fluorescence quantum yield of riboflavin derivatives is moderately high depending on the solvent polarity, pH, and the presence of different subunits in studied systems [18, 19]. Optical and HOMO-LUMO energy levels of flavin chromophores can be easily tuned by attaching substituents into heterocycle system [20]. In this regard, suitable molecular adjustments can be made to obtain suitable small organic molecule for organic photovoltaics. However, to the best of our knowledge, there have been no reports of BHJ-SC devices in which any riboflavin derivative was used as an acceptor component in their active layers.

In this study, we synthesized a neutral and a cationic riboflavin derivative, showing good solubility and giving low HOMO energy levels, in order to investigate their charge transport property and optoelectronic performance. We investigated the photophysical and electrochemical properties of chromophores in different solvents of polarities and also on thin films. Notably, we compared to their mobilities with each other measured under identical conditions.

Experimental Section

General Characterization Techniques

Solvents were purified and dried using standard techniques. ^{1}H NMR and ^{13}C NMR spectra were recorded on a Bruker spectrometer operating at 400 MHz, δ values are given in ppm (relative to TMS) and coupling constants (J) are reported in Hz. UV-Vis absorption spectra were recorded on a Perkin Elmer Lambda 950 spectrophotometer. Cyclic voltammetry (CV) measurements were performed using a CH instruments 660B–Electrochemical Workstation, wherein platinum acts as the counter electrode, an Ag/Ag$^+$ as the reference electrode, and a glassy carbon as the working electrode at a scan rate of 100 mV/s. Samples were prepared in acetonitrile solution with 0.1 M [TBA][PF6] as the electrolyte. The reference electrode was calibrated with an internal standard of ferrocene. Potentials were referenced to the ferrocenium/ferrocene redox couple with its oxidation potential detected at +0.66 V. HOMO, LUMO, and band gap values were calculated according to the eq. [21]:

$$E_{HOMO} = e\left(E_{ox}^{onset} + 4.8\right); E_{LUMO} = -e\left(E_{red}^{onset} + 4.8\right)$$
$$E_g^{opt} = {}^{1240}/_{\lambda_{abs}^{onset}}; E_{HOMO} = E_{LUMO} - E_g^{opt}$$

Fluorescence and time-resolved measurements were carried out with a commercial fluorimeter (FLS 920 Edinburg). The fluorescence decay times were measured by single photon counting method at excitation wavelength of 368.8 nm. Emission was at 550 nm detected at the magic angle relative to the vertically polarized beam. Data analysis was carried out using a nonlinear, exponential tail fit method [22]. The goodness-of-fit was judged from the reduced χ^2 ($\leq$ 1.2) [23] and weighted residuals. All measurements were performed in 1 cm optical path length quartz cuvettes. Non-contact mode atomic force microscopy (AFM) was performed with an Ambious Technology Q-Scope 250 Model instrument.

The minimum energy of geometry was performed in the framework of density functional theory (DFT) [24] by means of the B3LYP functional using the Gaussian 09 W program. The 6-31G(d) level [25] was chosen in order to display HOMO and LUMO orbitals for stable structures.

Materials

Acetic anhydride and 4-dimethylaminopyridine were purchased from Merck Company. Riboflavin, perchloric acid, N,N-dimethylformamide, dimethyl sulfoxide, potassium carbonate, and poly(3-hexylthiophene-2,5-diyl) (P3HT) were purchased from Sigma Aldrich. Also, 1,6-dibromohexane (Fluka) was used as received. Scheme 1 shows the synthetic pathway for **Rbf-II** and **Rbf-III** dyes.

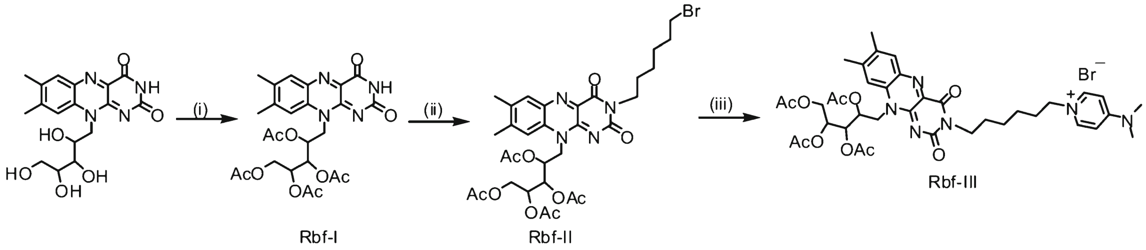

Scheme 1 Synthesis of **Rbf-(I-III)** dyes. (i) Acetic acid/Acetic anhydride (1:1 *v*/v), HClO$_4$, 45 °C [28]; (ii) 1,6-dibromohexane, DMF, K$_2$CO$_3$, room temperature [29]; (iii) DMSO, DMAP, room temperature

OPV Device Fabrication, Photovoltaic and Mobility Measurements

ITO glass substrates (from Delta Tech. Corp., 2.5 × 2.5 cm in size and with R_{sheet}: 10 Ω/sq. conductivity) were cleaned using the following sequential steps: rinsing with deionized water; sonication in acetone, and isopropanol for 15 min each; and drying with nitrogen. Finally, the substrates were treated with oxygen plasma for 5 min. A filtered suspension of PEDOT:PSS (AL4083) in water was spun cast at 4000 rpm for 30 s, followed by baking at 120 °C for 30 min in ambient. Solution processing of the active layers was performed under an inert-atmosphere in glovebox. The photoactive layers containing blends of P3HT and riboflavin dyes (mixing at concentrations of 2 wt%) in 1:1 and 1:2 mass ratios were spun cast from chloroform solution at 1000 rpm and, then dried at 120 °C for 30 min in a N_2 atmosphere. Finally, Al (100 nm) layer was deposited on top of the BHJ-SC by thermal evaporation with metal shadow mask in thermal evaporator equipped MBRAUN 200B glove box. All characterizations were done under inert atmosphere in glove box.

Space-charge-limited current (SCLC) measurements were measured on a device similar to BHJ-SC devices.

The current density − voltage (J − V) characteristics were investigated by using Keithley 2400 source meter under simulated AM1.5G illumination at 100 mW/cm^2 irradiance supplied by a MHG lamb (375 W) and, also in dark. The mobilities were determined by fitting the dark current using an equation given below:

$$J_{SCLC} = \frac{9}{8}\varepsilon_0\varepsilon_r\mu_e\frac{V^2}{L^3}$$

where ε_o is the permittivity of free space, ε_r is the dielectric constant of the riboflavin film, μ_e is the electron mobility, V is the applied voltage, and L is the thickness of the photo-active layer [26, 27].

Synthesis

*Synthesis of 2',3',4',5'-Tetraacetylriboflavin (**Rbf-I**)*

In a two-necked 50 mL Schlenk flask, riboflavin (0.5 g, 1.33 mmol) was added to a 40 mL of solution containing a mixture of glacial acetic acid and acetic anhydride in (v:v, 1:1) volume percent. After the dropwise addition of 100 μL of 70% perchloric acid, the mixture was stirred for 40 min at 45 °C. The mixture was cooled in an ice bath and diluted with an equal volume of water and, then solution was extracted with chloroform (3 × 25 mL). The combined organic extracts were washed with deionized water (3 × 25 mL), followed with a saturated solution of NaCl. The combined organic phases was evaporated to dryness and, then the product was recrystallized from 95% ethanol, yielding 80%. FT-IR (KBr pellet, cm^{-1}): 3158, 3032 (aromatic ν_{C-H}), 2812 (aliphatic ν_{C-H}), 1749 (ester $\nu_{C=O}$), 1663 (amide I. band $\nu_{C=O}$), 1577 (aromatic $\nu_{C=C}$), 1537 (amide II. band $\nu_{C=O}$), 1506, 1438, 1372, 1242, 1212, 1056, 839, 603 cm^{-1}. ^{1}H NMR (400 MHz, $CDCl_3$ δ 7.27 ppm): δ = 8.89 (1H, s), 8.00 (1H, s), 7.56 (1H, s), 5.66 (1H, d, J = 9.0 Hz), 5.47–5.38 (3H, m), 4.89 (1H, s), 4.42 (1H, dd, J_1 = 9.0 J_2 = 2.9 Hz), 4.26–4.21 (1H, m), 2.55 (3H, s), 2.43 (3H, s), 2.27 (3H, s), 2.20 (3H, s), 2.06 (3H, s), 1.74 (3H, s) ppm. ^{13}C NMR [100 MHz, $CDCl_3$ δ 77.4 (3 peaks)]: δ = 171.5, 171.2, 170.7, 170.6, 160.2, 155.4, 151.5, 137.6, 136.7, 135.2, 133.6, 116.2, 70.8, 69.7, 69.3, 62.1, 45.1, 21.5, 21.1, 20.8, 20.7, 20.3, 19.4 ppm.

*Synthesis of 2,3,4,5-Tetra-O-Acetyl-1-[3-(6-Bromohexyl) -7,8-Dimethyl-2,4-Dioxo-3,4-Dihydrobenzo[g] Pteridin-10(2H)-Yl]-1-Deoxypentitol (**Rbf-II**)*

To a solution of **Rbf-I** (0.1 g, 0.18 mmol) in 1.5 mL of dry N,N-dimethylformamide, potassium carbonate (40 mg, 0.29 mmol) was added in a single portion, and dark green suspension was stirred for 45 min at room temperature under an argon atmosphere. 1,6-dibromohexane (118 μl, 0.77 mmol) in 0.7 mL of N,N-dimethylformamide was added dropwise to the solution, and the mixture was stirred for 6 h at room temperature. Solution of dichloromethane:acetic acid (v:v, 9:1) volume percent was added to the mixture for neutralization and, then the organic phase was washed with equal volume of water and followed by a final washing with a saturated solution of NaCl. The organic layer was separated, dried over sodium sulfate, and evaporated to dryness. The product was purified by column

Table 1 Optical absorption wavelengths of **Rbf-II** and **Rbf-III** dyes in different solvents of polarities (λ (nm))

Dyes / Solvents	$CHCl_3$				THF				MeOH				MeCN			
	λ_1	λ_2	λ_3	λ_4^{a}	λ_1	λ_2	λ_3	λ_4^{a}	λ_1	λ_2	λ_3	λ_4^{a}	λ_1	λ_2	λ_3	λ_4^{a}
Rbf-II	479	450	348	275	472	445	341	270	472	447	355	273	472	444	345	274
Rbf-III	478	451	349	276	471	443	340	272	471	447	351	274	470	444	345	276

^{a} indicates the optical wavelength in which shows the highest absorption coefficient

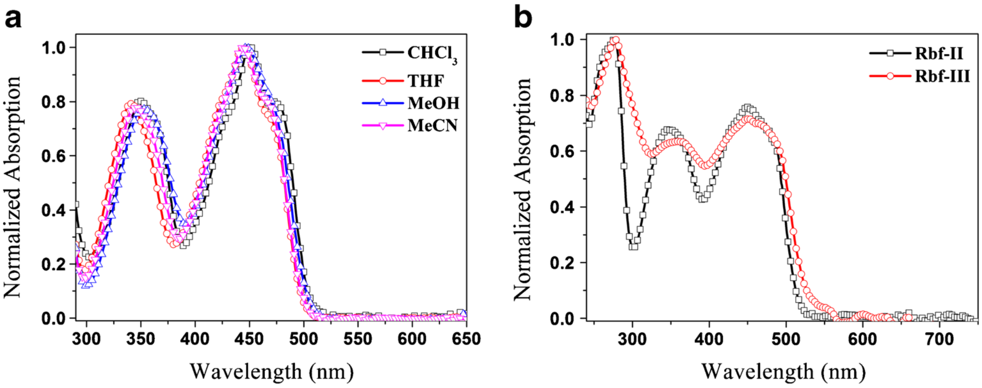

Fig. 1 **a** Normalized UV–Vis absorption spectra of **Rbf-II** dye in different solvent of polarities. **b** Comparison of normalized UV–Vis absorption spectra of **Rbf-II** and **Rbf-III** dyes coated on quartz substrates

chromatography eluting with chloroform:acetone (4:1), yielding 30%. FT-IR (NaCl disk, cm^{-1}): 2936, 2857 (aliphatic $\nu_{C\text{–}H}$), 1748 (ester $\nu_{C=O}$), 1709 (imide $\nu_{C=O}$), 1661 (amide I. band $\nu_{C=O}$), 1587 (aromatic $\nu_{C=C}$), 1551 (amide II. band $\nu_{C=O}$), 1435, 1371, 1219, 1049, 735, 601 cm^{-1}. ^{1}H NMR (400 MHz, CDCl$_3$ δ 7.26 ppm): δ = 8.01 (1H, s), 7.52 (1H, s), 5.66 (1H, d, J = 9.0 Hz), 5.50–5.34 (3H, m), 4.91 (1H, s), 4.43 (1H, dd, J_1 = 9.0 J_2 = 2.9 Hz), 4.26–4.21 (1H, m), 4.05 (2H, t, J = 7.6 Hz), 3.40 (2H, t, J = 6.8 Hz), 2.54 (3H, s), 2.43 (3H, s), 2.28 (3H, s), 2.21 (3H, s), 2.06 (3H, s), 1.87 (3H, m), 1.72 (3H, s), 1.52–1.38 (5H, m) ppm. ^{13}C NMR [100 MHz, CDCl$_3$ δ 77.4 (3 peaks)]: δ = 171.5, 171.2, 170.7, 170.5, 160.5, 155.8, 137.2, 136.5, 135.3, 133.6, 115.9, 70.8, 69.3, 62.2, 44.7, 42.0, 33.9, 32.8, 27.9, 27.6, 26.2, 21.4, 21.1, 20.8, 20.7, 20.3, 19.4 ppm.

*Synthesis of 2,3,4,5-Tetra-O-Acetyl-1-Deoxy-1-[3-{6-[4-(Dimethylamino)Pyridinium-1-Yl]Hexyl}-7,8-Dimethyl-2,4-Dioxo-3,4-Dihydrobenzo[g]Pteridin-10(2H)-Yl]Pentitol Bromide (***Rbf-III***)*

Rbf-II (40 mg, 56.5 μmol) was dissolved in 0.5 mL of DMSO, and the solution was added to 4-dimethylaminopyridine (DMAP, 20 mg, 0.16 mmol) in DMSO (2 mL) slowly. The resulting mixture was stirred at room temperature under an argon atmosphere. The crude product was purified by flash chromatography using chloroform:methanol as eluent (from 5:0 to 4:1 by v:v volume), yielding 40%. FT-IR (NaCl disk, cm^{-1}): 3417, 2955, 2868 (aliphatic $\nu_{C\text{–}H}$), 1746 (ester $\nu_{C=O}$), 1707 (imide $\nu_{C=O}$), 1650 (amide I. band $\nu_{C=O}$), 1585 (aromatic $\nu_{C=C}$), 1549

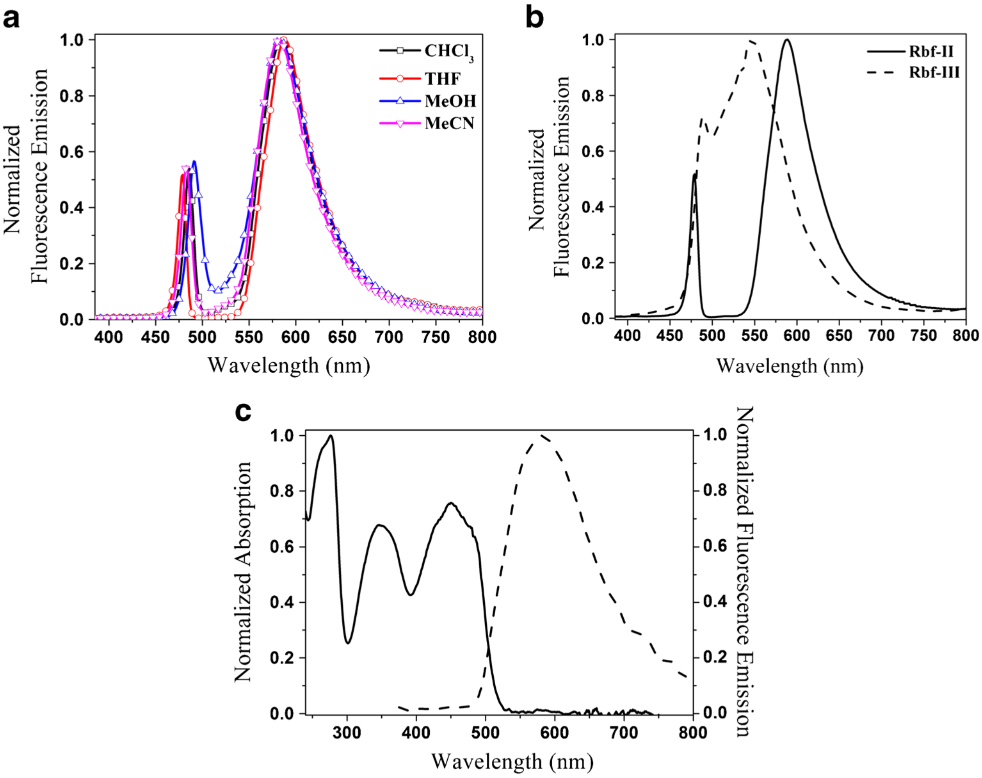

Fig. 2 **a** Normalized fluorescence emission spectra of **Rbf-II** dye in different solvent of polarities. **b** Comparison of normalized fluorescence emission spectra of **Rbf-II** and **Rbf-III** dyes in THF. **c** Comparison of normalized fluorescence emission and UV–Vis absorption spectra of **Rbf-II** dye coated on quartz substrates (λ_{exc} = 365 nm)

Table 2 Long-wavelength fluorescence emissions (λ_{em} (nm)), fluorescence quantum yields (Φ_F)[a] and fluorescence decay times (τ_f (ns)) with their fit values of **Rbf-II** and **Rbf-III** dyes in different solvents of polarities (λ_{exc} = 365 nm)

Dyes / Solvents	$CHCl_3$				THF				MeOH				MeCN			
	λ_{em}	Φ_F	χ^2	τ_f	λ_{em}	Φ_F	χ^2	τ_f	λ_{em}	Φ_F	χ^2	τ_f	λ_{em}	Φ_F	χ^2	τ_f
Rbf-II	585	0.88	0.77	6.40	588	0.64	0.88	6.62	583	0.78	0.76	5.73	583	0.64	0.86	6.15
Rbf-III	575	0.83	0.79	5.81	546	0.88	1.18	5.53	577	0.85	0.81	5.57	575	0.71	0.80	6.08

[a] Fluorescence quantum yields have been determined using quinine sulfate dihydrate (λ_{exc} = 365 nm, Φ_F = 0.546, 1 N H_2SO_4) [32]

(amide II. band $\nu_{C=O}$), 1433, 1370, 1228, 1048, 843, 735, 601 cm^{-1}. ^1H NMR (400 MHz, $CDCl_3$ δ 7.26 ppm): δ = 8.40 (d, J = 6.2 Hz, 2H), 7.99 (s, 1H), 7.54 (s, 1H), 7.01 (d, J = 6.2 Hz, 2H), 5.65 (s, 1H), 5.41 (m, 3H), 4.93 (s, 1H), 4.44 (dd, J = 12.3, 2.7 Hz, 1H), 4.30 (t, J = 6.0 Hz, 2H), 4.22 (d, J = 6.6 Hz, 1H), 4.04–3.99 (m, 2H), 3.26 (s, 6H), 2.54 (s, 3H), 2.42 (s, 3H), 2.25 (s, 3H), 2.19 (s, 3H), 2.05 (s, 3H), 1.88 (t, J = 6.0 Hz, 2H), 1.71 (s, 3H), 1.38 (m, 4H), 1.24 (m, 2H) ppm.

Results and Discussion

Steady State and Time Resolved Measurements

Riboflavin molecule can give a limited number of chemical reactions due to its instability under high pH conditions. It is also known that its structure decomposes considerably to lumichrome and lumiflavin chromophores by removing of polyribitol functional group when exposed to light in basic solution [30]. We increased the stability of riboflavin through esterification reaction of poly hydroxyl groups giving stable tetraacetylriboflavin (**Rbf-I**) molecule. Then, solubility of riboflavin was improved by attaching long chain hexyl group to imide nitrogen, giving **Rbf-II** dye. To investigate cationic effects of riboflavin on charge separation and optoelectronic performance, **Rbf-II** and **Rbf-III** dyes were synthesized according to the procedure reported in previous literature [29].

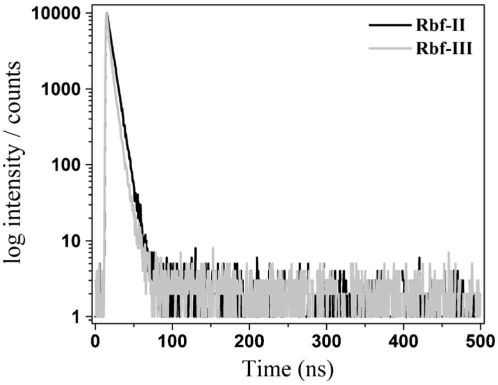

Fig. 3 Comparison of fluorescence decay analysis of **Rbf-II** and **Rbf-III** dyes in THF solution ($\lambda_{detection}$ = 550 nm)

Both **Rbf-II** and **Rbf-III** dyes show two distinct absorption bands around 345 nm and 445 nm, and a small shoulder centered around 475 nm in studied solutions, as given in Table 1. The lowest energy absorption are mainly attributed to charge transfer complex between lumichrome and ribityl groups. The others are contributed to $n-\pi^*$ and $\pi-\pi^*$ transitions of lumichrome ring [31]. DMAP substitution at the end of alkyl chain has much less impact on spectral shift, which is proved by the similar absorption values for **Rbf-II** and **Rbf-III** dyes in solution. Compared with THF, MeOH, and MeCN in Fig. 1a, **Rbf-II** dye in $CHCl_3$ has slightly optical larger bandgap probably due to its more relaxation behavior causing the more planar conformation of lumichrome in $CHCl_3$ solvent. When the UV-Vis spectra of **Rbf-II** and **Rbf-III** dyes in the film state are compared, as shown in Fig. 1b, **Rbf-II** absorbs the light at 453 and 351 with the maximum absorption value at 278 nm while **Rbf-III** shows slight red shifts giving the absorptions at 463 and 357 nm in the film state.

Figure 2a illustrates the fluorescence emission spectra of **Rbf-II** dye in different solvents, and other photophysical properties of both dyes are summarized in Table 2. **Rbf-II** dye brings about two emission bands, one of which is observed around 585 nm, and the other one, minor band, is observed at 485 nm. **Rbf-III** dye exhibits a broader emission band with a blue-shift of 42 nm as compared to **Rbf-II** in THF solution, as illustrated in Fig. 2b. When excited at 365 nm, lumichrome-related absorption band, both dyes display

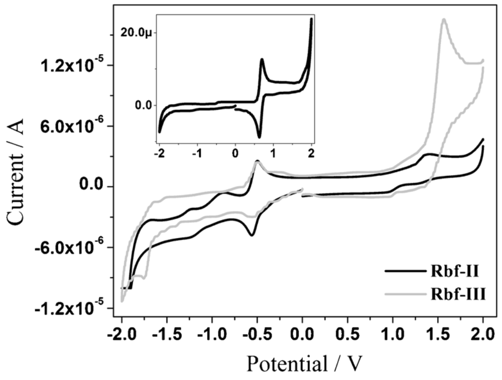

Fig. 4 Cyclic voltammograms of **Rbf-II** and **Rbf-III** dyes on glassy carbon working electrode in 0.1 M [TBA][PF6]/Me-CN (Scan rate: 100 mV s^{-1}). Inset shows the cyclic voltammograms of internal reference (ferrocene) under the same conditions

Table 3 Electrochemical values and HOMO-LUMO energies of **Rbf-II** and **Rbf-III** dyes with respect to the vacuum level

Dyes	E^0_{red3} (V)	E^0_{red2} (V)	E^0_{red1} (V)	E^0_{ox1} (V)	LUMO (eV)	HOMO (eV)	E_{0-0}^{a}(eV) (abs)
Rbf-II	−1.24	−0.86	−0.53	1.35	−3.61	−5.98	2.37
Rbf-III	-	−1.75	−0.52	1.56	−3.62	−5.96	2.34

[a] The zeroth–zeroth transition $E_{0–0}$ values were estimated from the intersection of the apsis and the straight line which is drawn from the red side of the UV-Vis absorption band of their thin films

characteristic emission features of lumichrome main core around 485 nm [31]. Other major band, observed around 585 nm, indicates the emission character of a charge transfer complex generated from the interaction between lumichrome and polyribitol group of riboflavin. Fig. 2c gives an outlook of absorption and emission spectra of **Rbf-II** on quartz substrate. The shapes of fluorescence emission spectrum for **Rbf-II** on thin film seems to be combined and slightly broader as compared to that of solution phase. Lumichrome emission could not be observed in Fig. 2c. This may be attributed to emission quenching of lumichrome resulted from the solid-state packing of aromatic rings in thin film. The thin film state of **Rbf-II** dye has showed a unique packing motif as compared to the solution state, which led to unique properties in its emission and absorption spectra.

Fluorescence quantum distributions of **Rbf-II** and **Rbf-III** dyes in the studied solvents are reported in Table 2. Fluorescence quantum yields (Φ_F) of **Rbf-II** and **Rbf-III** dyes evaluated using quinine sulfate dihydrate as reference were calculated to be in the range of 0.64–0.88. These values are reasonably high when compared to Φ_F values for pristine riboflavin reported in the literature (Φ_F: 0.21–0.39, given in common organic solvents) [19, 33]. It is also reported that 3-methyl-riboflavin tetraacetate structure has much lower fluorescence quantum yields (Φ_F: 0.064–0.12, given in common organic solvents) as compared to that of riboflavin. Sikorski, et al. proposed that 3-methyl-riboflavin tetraacetate forms a crystal packing model which consists of intermolecular C–H· · ·O hydrogen bonds between C-11 hydrogen and carbonyl oxygen atoms in the structure [34]. In our synthesized riboflavin dyes, this kind of hydrogen bonding may be inhibited because of long hexyl chain attached to N-3 atom. Each emissive lumichrome rings are separated from each other so that lumichrome gives its own emission band around 485 nm (see Fig. 2b). Finally, our synthesized **Rbf-II** and **Rbf-III** dyes gained an extra emission of lumichrome resulting much higher Φ_F values as compared to that of 3-methyl-riboflavin tetraacetate. Also, **Rbf-III** gave much higher Φ_F values as compared to that of **Rbf-II** in the studied organic solvents, except $CHCl_3$. Attaching of pyridinium salt in **Rbf-III** dye gave an extra contribution to total Φ_F value. Different pyridinium salts are in progress for use as fluorescent chemosensors in the literature [35, 36].

In time-resolved experiments, analysis of the decays revealed mono-exponential decays at detected emission wavelength of 550 nm for **Rbf-II** and **Rbf-III** dyes in common organic solvents as given in Table 2. Figure 3 compares the fluorescence decays of the dyes in THF solution. The calculated fluorescence lifetimes were found to be with the range of 5.53–6.62 ns for **Rbf-II** and **Rbf-III** dyes, and in good agreements with those reported in the literature for 3-methyl-riboflavin tetraacetate at values between 4.4 and 5.8 ns [34]. Actually, fluorescence decay time for lumichrome were reported below 1 ns in organic solvents [31]. These much higher values for **Rbf-II** and **Rbf-III** dyes may be attributed to the stationary fluorescence of charge transfer complex defined for riboflavin structure.

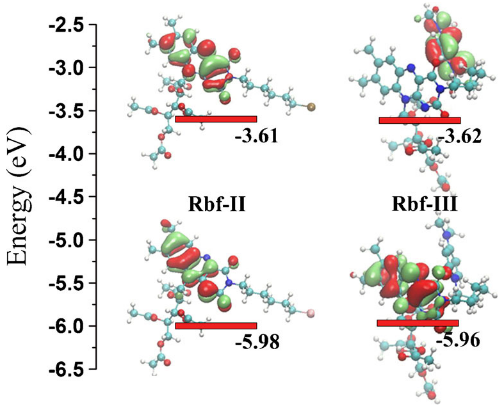

Fig. 5 Optimised ground-state geometries and frontier orbital energies of compounds **Rbf-II** and **Rbf-III** dyes obtained by DFT calculations

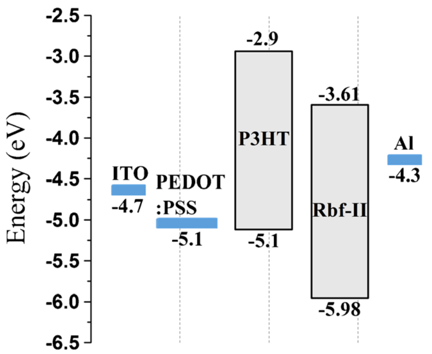

Fig. 6 Matching of electronic energy levels of BHJ-SC components including **Rbf-II** as acceptor part

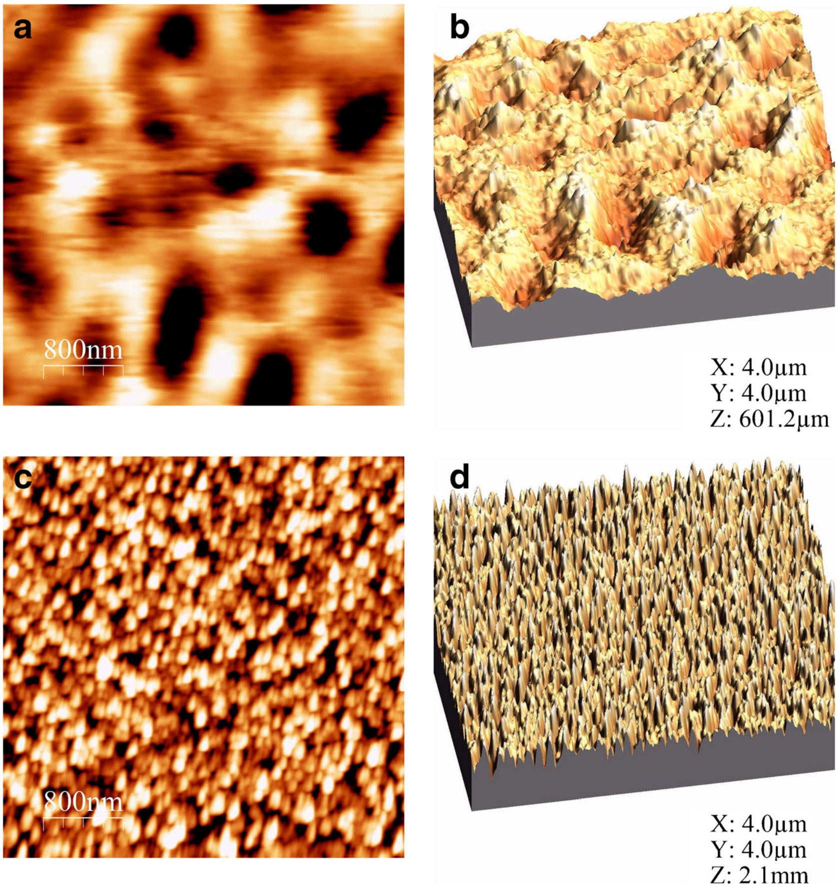

Fig. 7 AFM images (4 µm × 4 µm) of **a, b Rbf-II** and **c, d Rbf-III** films spin-coated from chloroform solution

CV Measurements and DFT Calculations

Solution phase cyclic voltammograms (CV) of riboflavin dyes were investigated in order to estimate their energy levels. Fig. 4 shows CVs of **Rbf-II** and **Rbf-III** dyes on Pt electrode with 0.1 M [TBA][PF6]/Me-CN as the electrolyte at a scan rate of 100 mV s^{-1}. While **Rbf-II** exhibits three reduction waves at −0.53, −0.86, and −1.24 V, reduction processes for **Rbf-III** are slightly shifted to more negative region giving two reduction waves at −0.52 and −1.75 V, as summarized in Table 3. Tetraacetic acid contributes to the reduction potential of the structures by its electron-withdrawing nature. The first reduction waves for both dyes may be attributed to reduction of lumichrome-carbonyl group giving one electron reduction to form the radical anion of riboflavin (Rbf$^{\bullet-}$). Variable scan rate CV experiments of riboflavin in DMSO by Webster et al. [37] have revealed that this radical anion generates Rbf^{2-} anion with accepting one more electron to nitrogen atom giving reduction at much lower negative reduction potentials for **Rbf-II** and **Rbf-III**. It is noted that **Rbf-III** gives much lower negative reduction potential at −1.75 V resulting from electron-withdrawing effect of pyridinium salts. As illustrated in Fig. 5, both HOMO and LUMO frontiers orbitals of **Rbf-II** indicated significant delocalization over the central lumichrome core with no any contribution from the side ribityl group. Pyridinium moiety in the optimized geometry of **Rbf-III** is located at opposite side of lumichrome rings. The LUMO orbitals of **Rbf-III** spread over the pyridinium unit and extend into the mainly nitrogen cation side, whereas HOMO level is completely delocalized over the whole lumichrome rings. The reduction potential of **Rbf-III** at −1.75 V may be caused by one-electron reduction of the LUMO which is probably located on pyridinium cation.

HOMO levels of **Rbf-II** and **Rbf-III** dyes are calculated to be about −5.98 eV and −5.96 eV, respectively, which are more

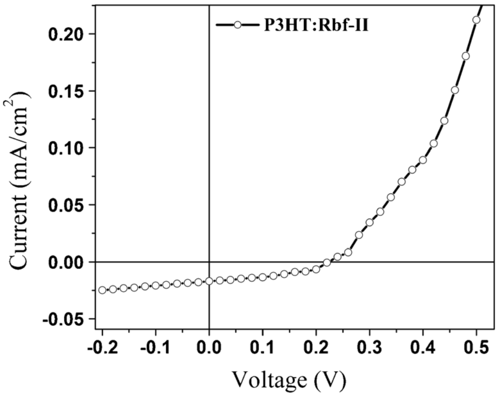

Fig. 8 J-V curve of photovoltaic device using P3HT:**Rb-II** blend as active layer

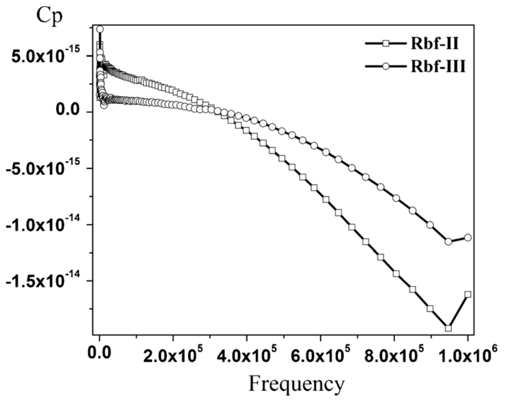

Fig. 9 The variations in the capacitance-frequency (C-F) characteristic of FTO/TiO_2/**Rbf-II** or **Rbf-III**/LiCl/Al devices

close to that of well-known PCBM acceptor for BHJ-SC devices [38]. Their appropriate energy levels and bandgaps of 2.37 and 2.34 eV for **Rbf-II** and **Rbf-III**, respectively, and combined with the high molar absorption coefficients suggest that these flavin derivatives might be good candidates as n-type acceptors, possibly for organic solar cells. Their bandgaps also could be well matched with higher bandgap polymers such as P3HT, as shown in Fig. 6.

AFM Images and Optoelectronic Measurements

Figure 7 shows the film morphologies of compounds **Rbf-II** and **Rbf-III** from chloroform solutions. Compound **Rbf-II** with R = n-$C_6H_{12}Br$ exhibits no distinguished high-ordered structure (Fig. 7a and b). Similarly, in compound **Rbf-III**, where bromide group replaced with pyridinium salt functionality, very small ordered domains are detectable (Fig. 7c). Salt effect of pyridinium on the organization of riboflavin dye at macroscopic order within the film is observed in Fig. 7d. Average roughness of thin films for compounds **Rbf-II** and **Rbf-III** are around 3.330 and 4.355 nm, respectively.

The photovoltaic performances of **Rbf-II** and **Rbf-III** dyes were investigated in conventional device configuration of ITO/PEDOT:PSS/P3HT:**Rbf-II** or **Rbf-III**)/Al(100 nm). The J–V curves of optimized device based on **Rbf-II** with P3HT were illustrated in Fig. 8. While the best **Rbf-II**:P3HT-based device shows a J_{sc} of 5×10^{-3} mA·cm^{-2}, a V_{oc} of 80 mV, and a FF of 0.30, resulting in an overall PCE of 1.2×10^{-4}%, **Rbf-III**:P3HT-based device could not give any current. Generally, used dyes on film state may lead to the formation of uniform active layer which is one of the possible reasons for low cell efficiencies.

Additionally, in order to understand the effect of charge transport properties on the obtaining of poor photocurrent values, electron mobilities were measured using the devices fabricated with the configuration of FTO/TiO_2(40 nm)/**Rbf-II** or **Rbf-III**(60 nm)/LiF(0.6 nm)/Al(70 nm) using the SCLC method. The capacitance-frequency (C-F) characteristics of the devices were given in Fig. 9. Charge collection of **Rbf-III** is lower at low frequencies, which is the indication of the presence of conductive surface or tunneling paths, possible arising from the ionic behavior of pyridinium group. Also, dark current density-effective voltage characteristics of SCLC mobility for active layer **Rbf-II** and **Rbf-III** were given in Fig. 10a and Fig. 10b, respectively. The electron mobilities of **Rbf-II** and **Rbf-III** dyes were calculated to be about 1.3×10^{-3} and 9.0×10^{-6} cm^2/V·s, respectively. These results clarify the reason of very low conversion efficiency with **Rbf-III**. The lower electron mobility of **Rbf-III** might be caused by the electron deficient nature of pyridinium salt acting as electron-trapping sites to interrupt the charge-carrier transportation. Even if the poor cell efficiencies of these riboflavin-derived compounds, we can improve the charge transport properties of riboflavin core by making similar modifications in its structure in future works.

Conclusion

We synthesized two natural organic small molecules (**Rbf-II** and **Rbf-III**) that consisted of riboflavin as the central core luminophore structure and n-hexyl as the terminal alkyl group. **Rbf-II** and **Rbf-III** dyes have broad absorption bands covering 300–550 nm wavelength range with bandgaps of

Fig. 10 Dark current density-effective voltage characteristics of SCLC mobilities in **a** FTO/TiO_2/**Rbf-II**/LiCl/Al and **b** FTO/TiO_2/**Rbf-III**/LiCl/Al devices

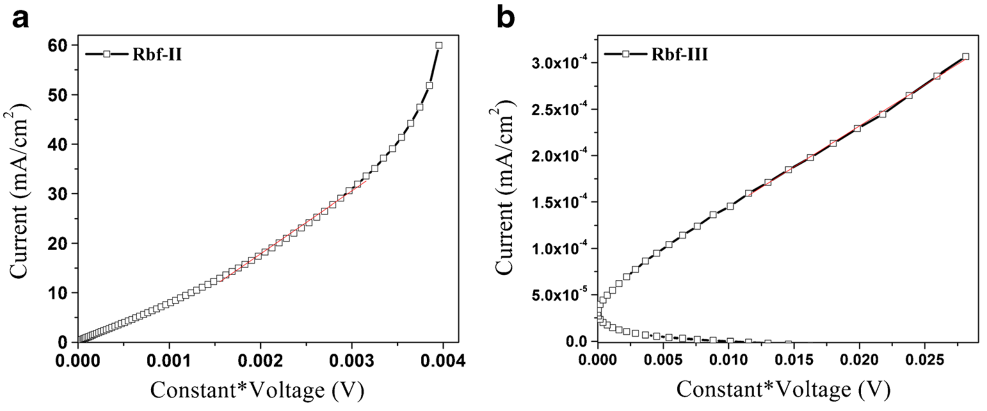

approximately 2.3 eV and relatively low HOMO energy levels around −5.9 eV. This is energetically suitable position indicating hole transfer from the dyes to polymer donor in BHJ-SC devices. Pyridinium substituent of **Rbf-III** narrows the band gap of riboflavin to 2.34 eV and improves the electron acceptor property of the structure.

One of the major findings of this work is that photophysical and charge transport properties of riboflavin core can be modified significantly attaching with different substituents. This study reveals that optical and charge-transport properties of neutral riboflavin structure with long alkyl chain encourage the synthesis of new riboflavin derivatives for organic photovoltaic applications. Similar modifications on riboflavin structure can give some insights into its potential usage in more favorable optoelectronic materials.

Acknowledgements This work was supported by the Scientific and Technological Research Council of Turkey (TUBITAK) with the project number of 113Z250. We thank to Ege University for the support of the use of Gaussian 09 W programme for DFT calculations.

References

1. Lu CY, Wang WF, Lin WZ, Han ZH, Yao SD, Lin NY (1999) Generation and photosensitization properties of the oxidized radical of riboflavin: a laser flash photolysis study. J Photoch Photobio B 52:111–116
2. Lu CY, Lin WZ, Wang WF, Han ZH, Yao S, Lin NY (2000) Riboflavin (VB2) photosensitized oxidation of 2′-deoxyguanosine-5′-monophosphate (dGMP) in aqueous solution: a transient intermediates study. PCCP Phys Chem Ch Ph 2:329–334
3. Alva S, Phadke RS (1995) Riboflavın - a potential material for molecular electronics applications. Biosystems 35:153–156
4. Andrés-Lacueva C, Mattivi F, Tonon D (1998) Determination of riboflavin, flavin mononucleotide and flavin–adenine dinucleotide in wine and other beverages by high-performance liquid chromatography with fluorescence detection. J Chromatogr A 823:355–363
5. Insinska-Rak M, Golczak A, Sikorski M (2012) Photochemistry of riboflavin derivatives in methanolic solutions. J Phys Chem A 116: 1199–1207
6. Choe E, Huang R, Min DB (2005) Chemical reactions and stability of riboflavin in foods. J Food Sci 70:R28–R36
7. Lee YH, Lee J, Min DB, Pascall MA (2014) Effect of riboflavin on the photo-oxidative stability of vegetable oil in salad dressing. Food Chem 152:349–354
8. Khaydukov EV, Mironova KE, Semchishen VA, Generalova AN, Nechaev AV, Khochenkov DA, Stepanova EV, Lebedev OI, Zvyagin AV, Deyev SM, Panchenko VY (2016) Riboflavin photoactivation by upconversion nanoparticles for cancer treatment. Sci Rep 6:351031–351039
9. Maisch T, Eichner A, Spath A, Gollmer A, Konig B, Regensburger J, Baumler W (2014) Fast and effective photodynamic inactivation of multiresistant bacteria by cationic riboflavin derivatives. PLoS one 9: e111792(1−8)
10. Zirak P, Penzkofer A, Mathes T, Hegemann P (2009) Photodynamics of roseoflavin and riboflavin in aqueous and organic solvents. Chem Phys 358:111–122
11. Silva AV, López-Sánchez A, Junqueira HC, Rivas L, Baptista MS, Orellana G (2015) Riboflavin derivatives for enhanced photodynamic activity against Leishmania parasites. Tetrahedron 71:457–462
12. Challier C, Mártire DO, García NA, Criado S (2017) Visible light-mediated photodegradation of imidazoline drugs in the presence of riboflavin: possible undesired effects on imidazoline-based eye drops. J Photoch Photobio A 332:399–405
13. Abdel-Fattah TM, Ebrahim S, Soliman M, Hafez M (2013) Dye-sensitized solar cells based on polyaniline-single wall carbon nanotubes composite. Ecs J Solid State Sc 2:M13–M16
14. Ebrahim S, Soliman M, Anas M, Hafez M, Abdel-Fattah T (2013) Dye-sensitized solar cell based on polyaniline/multiwalled carbon nanotubes counter electrode. Int J Photoenergy 2013:906820(1−6)
15. Mollahosseini M, Karunaratne E, Gibson GN, Gascon JA, Papadimitrakopoulos F (2016) Fullerene-assisted photoinduced charge transfer of single-walled carbon nanotubes through a flavin helix. J Am Chem Soc 138:5904–5915
16. Yu X, Eymur S, Singh V, Yang B, Tonga M, Bheemaraju A, Cooke G, Subramani C, Venkataraman D, Stanley RJ, Rotello VM (2012) Flavin as a photo-active acceptor for efficient energy and charge transfer in a model donor-acceptor system. Phys Chem Chem Phys 14:6749–6754
17. Murakami M, Ohkubo K, Fukuzumi S (2010) Inter- and intramolecular photoinduced electron transfer of flavin derivatives with extremely small reorganization energies. Chem-Eur J 16:7820–7832
18. Drössler P, Holzer W, Penzkofer A, Hegemann P (2002) pH dependence of the absorption and emission behaviour of riboflavin in aqueous solution. Chem Phys 282:429–439
19. Tyagi A, Zirak P, Penzkofer A, Mathes T, Hegemann P, Mack M, Ghisla S (2009) Absorption and emission spectroscopic characterisation of 8-amino-riboflavin. Chem Phys 364:19–30
20. Legrand YM, Gray M, Cooke G, Rotello VM (2003) Model systems for flavoenzyme activity: relationships between cofactor structure, binding and redox properties. J Am Chem Soc 125:15789–15795
21. Pommerehne J, Vestweber H, Guss W, Mahrt RF, Bassler H, Porsch M, Daub J (1995) Efficient 2-layer leds on a polymer blend basis. Adv Mater 7:551–554
22. Knutson JR, Beechem JM, Brand L (1983) Simultaneous analysis of multiple fluorescence decay curves - a global approach. Chem Phys Lett 102:501–507
23. Zuker M, Szabo AG, Bramall L, Krajcarski DT, Selinger B (1985) Delta-function convolution method (dfcm) for fluorescence decay experiments. Rev Sci Instrum 56:14–22
24. Frisch MJ, Trucks GW, Schlegel HB, Scuseria GE, Robb MA, Cheeseman JR, Scalmani G, Barone V, Mennucci B, Petersson GA, Nakatsuji H, Caricato M, Li X, Hratchian HP, Izmaylov AF, Bloino J, Zheng G, Sonnenberg JL, Hada M, Ehara M, Toyota K, Fukuda R, Hasegawa J, Ishida M, Nakajima T, Honda Y, Kitao O, Nakai H, Vreven T, Montgomery Jr. JA, Peralta JE, Ogliaro F, Bearpark MJ, Heyd J, Brothers EN, Kudin KN, Staroverov VN, Kobayashi R, Normand J, Raghavachari K, Rendell AP, Burant JC, Iyengar SS, Tomasi J, Cossi M, Rega N, Millam NJ, Klene M, Knox JE, Cross JB, Bakken V, Adamo C, Jaramillo J, Gomperts R, Stratmann RE, Yazyev O, Austin AJ, Cammi R, Pomelli C, Ochterski JW, Martin RL, Morokuma K, Zakrzewski VG, Voth GA, Salvador P, Dannenberg JJ, Dapprich S, Daniels AD, Farkas Ö, Foresman JB, Ortiz JV, Cioslowski J, Fox DJ. Gaussian 09. Wallingford, CT, USA: Gaussian, Inc.; 2009
25. Kohn W, Sham LJ (1965) Self-consistent equations including exchange and correlation effects. Phys Rev 140:A1133–A1138
26. Goh C, Kline RJ, Mcgehee MD, Kadnikova EN, Frechet JMJ (2005) Molecular-weight-dependent mobilities in regioregular poly(3-hexyl-thiophene) diodes. Appl Phys Lett 86:122110(1–3)

27. Carbone A, Kotowska BK, Kotowski D (2005) Space-charge-limited current fluctuations in organic semiconductors. Phys rev Lett 95:236601(1–4)
28. Ogasawara FK, Wang YL, Bobbitt DR (1992) Dynamically modified, biospecific optical fiber sensor for riboflavın binding-protein based on hydrophobically associated 3-octylriboflavin. Anal Chem 64:1637–1642
29. Di Meo C, Montanari E, Manzi L, Villani C, Coviello T, Matricardi P (2015) Highly versatile nanohydrogel platform based on riboflavin-polysaccharide derivatives useful in the development of intrinsically fluorescent and cytocompatible drug carriers. Carbohyd Polym 115:502–509
30. Sheraz MA, Kazi SH, Ahmed S, Anwar Z, Ahmad I (2014) Photo, thermal and chemical degradation of riboflavin. Beilstein J Org Chem 10:1999–2012
31. Moyon NS, Mitra S (2011) Fluorescence solvatochromism in lumichrome and excited-state tautomerization: a combined experimental and DFT study. J Phys Chem A 115:2456–2464
32. Brouwer AM (2011) Standards for photoluminescence quantum yield measurements in solution (IUPAC technical report). Pure Appl Chem 83:2213–2228
33. Sun M, Moore TA, Song P-S (1972) Molecular luminescence studies of flavines. I Excited states of flavines J Am Chem Soc 94: 1730–1740
34. Insińska-Rak M, Sikorska E, Bourdelande JL, Khmelinskii IV, Prukała W, Dobek K, Karolczak J, Machado IF, Ferreira LFV, Dulewicz E, Komasa A, Worrall DR, Kubicki M, Sikorski M (2007) New photochemically stable riboflavin analogue—3-methyl-riboflavin tetraacetate. J Photoch Photobio A 186:14–23
35. Narang U, Zhao CF, Bhawalkar JD, Bright FV, Prasad PN (1996) Characterization of a new solvent-sensitive two-photon-induced fluorescent (aminostyryl)pyridinium salt dye. J Phys Chem-US 100:4521–4525
36. Turkewitsch P, Darling GD, Powell WS (1998) Enhanced fluorescence of 4-(p-dimethylaminostyryl)pyridinium salts in the presence of biological macromolecules. J Chem Soc Faraday Trans 94:2083–2087
37. Tan SL, Webster RD (2012) Electrochemically induced chemically reversible proton-coupled electron transfer reactions of riboflavin (vitamin B2). J Am Chem Soc 134:5954–5964
38. Scharber MC, Mühlbacher D, Koppe M, Denk P, Waldauf C, Heeger AJ, Brabec CJ (2006) Design rules for donors in bulk-heterojunction solar cells—towards 10% energy-conversion efficiency